Research Article | Vol. 8, No. 10 | 1 Oct 2017 | BIOMEDICAL OPTICS EXPRESS 4361
Biomedical Optics EXPRESS

Angle-selective optical filter for highly sensitive reflection photoplethysmogram

CHAN-SOL HWANG, SUNG-PYO YANG, KYUNG-WON JANG, JUNG-WOO PARK, AND KI-HUN JEONG*

Department of Bio and Brain Engineering and KAIST Institute for Health Science and Technology, Korea Advanced Institute of Science and Technology (KAIST), 291 Daehak-ro, Yuseong-gu, Daejeon, 34141, South Korea
kjeong@kaist.ac.kr

Abstract: We report an angle-selective optical filter (ASOF) for highly sensitive reflection photoplethysmography (PPG) sensors. The ASOF features slanted aluminum (Al) micromirror arrays embedded in transparent polymer resin, which effectively block scattered light under human tissue. The device microfabrication was done by using geometry-guided resist reflow of polymer micropatterns, polydimethylsiloxane replica molding, and oblique angle deposition of thin Al film. The angular transmittance through the ASOF is precisely controlled by the angle of micromirrors. For the mirror angle of 30 degrees, the ASOF accepts an incident light between - 90 to + 50 degrees and the maximum transmittance at - 55 degrees. The ASOF exhibits the substantial reduction of both the in-band noise of PPG signals over a factor of two and the low-frequency noise by three times. Consequently, this filter allows distinguishing the diastolic peak that allows miscellaneous parameters with diverse vascular information. This optical filter provides a new opportunity for highly sensitive PPG monitoring or miscellaneous optical tomography.

OCIS codes: (120.5240) Photometry; (220.4000) Microstructure fabrication; (230.3990) Micro-optical devices; (170.3890) Medical optics instrumentation;

References and links

1. J. Allen, "Photoplethysmography and its application in clinical physiological measurement," Physiol. Meas. **28**(3), R1–R39 (2007).
2. P. J. Chowienczyk, R. P. Kelly, H. MacCallum, S. C. Millasseau, T. L. G. Andersson, R. G. Gosling, J. M. Ritter, and E. E. Anggård, "Photoplethysmographic Assessment of Pulse Wave Reflection: blunted response to endothelium-dependent beta2-adrenergic vasodilation in type II diabetes mellitus," J. Am. Coll. Cardiol. **34**(7), 2007–2014 (1999).
3. M. Elgendi, "On the Analysis of Fingertip Photoplethysmogram Signals," Curr. Cardiol. Rev. **8**(1), 14–25 (2012).
4. K. Takazawa, N. Tanaka, M. Fujita, O. Matsuoka, T. Saiki, M. Aikawa, S. Tamura, and C. Ibukiyama, "Assessment of Vasoactive Agents and Vascular Aging by the Second Derivative of Photoplethysmogram Waveform," Hypertension **32**(2), 365–370 (1998).
5. H. H. Asada, P. Shaltis, A. Reisner, S. Rhee, and R. C. Hutchinson, "Mobile Monitoring with Wearable Photoplethysmographic Biosensors," IEEE Eng. Med. Biol. Mag. **22**(3), 28–40 (2003).
6. W. B. Murray and P. A. Foster, "The Peripheral Pulse Wave: Information Overlooked," J. Clin. Monit. **12**(5), 365–377 (1996).
7. J. C. Dorlas and J. A. Nijboer, "Photo-electric Plethysmography as a Monitoring Device in Anaesthesia. Application and interpretation," Br. J. Anaesth. **57**(5), 524–530 (1985).
8. E. C.-P. Chua, S. J. Redmond, G. McDarby, and C. Heneghan, "Towards Using Photo-plethysmogram Amplitude to Measure Blood Pressure During Sleep," Ann. Biomed. Eng. **38**(3), 945–954 (2010).
9. S. C. Millasseau, R. P. Kelly, J. M. Ritter, and P. J. Chowienczyk, "Determination of Age-related Increases in Large Artery Stiffness by Digital Pulse Contour Analysis," Clin. Sci. **103**(4), 371–377 (2002).
10. S. Lu, H. Zhao, K. Ju, K. Shin, M. Lee, K. Shelley, and K. H. Chon, "Can Photoplethysmography Variability Serve as an Alternative Approach to Obtain Heart Rate Variability Information?" J. Clin. Monit. Comput. **22**(1), 23–29 (2008).
11. A. A. Awad, A. S. Haddadin, H. Tantawy, T. M. Badr, R. G. Stout, D. G. Silverman, and K. H. Shelley, "The Relationship Between the Photoplethysmographic Waveform and Systemic Vascular Resistance," J. Clin. Monit. Comput. **21**(6), 365–372 (2007).

#296882 https://doi.org/10.1364/BOE.8.004361
Journal © 2017 Received 30 May 2017; revised 25 Aug 2017; accepted 28 Aug 2017; published 7 Sep 2017

Biomedical Optics EXPRESS

12. T. Tamura, Y. Maeda, M. Sekine, and M. Yoshida, "Wearable Photoplethysmographic Sensors-Past and Present," Electronics (Basel) **3**(2), 282–302 (2014).
13. C. Zhou, J. Feng, J. Hu, and X. Ye, "Study of Artifact-Resistive Technology Based on a Novel Dual Photoplethysmography Method for Wearable Pulse Rate Monitors," J. Med. Syst. **40**(3), 56 (2016).
14. K. M. Warren, J. R. Harvey, K. H. Chon, and Y. Mendelson, "Improving Pulse Rate Measurements during Random Motion Using a Wearable Multichannel Reflectance Photoplethysmograph," Sensors (Basel) **16**(3), 342 (2016).
15. M. R. Ram, K. V. Madhav, E. H. Krishna, N. R. Komalla, and K. A. Reddy, "A Novel Approach for Motion Artifact Reduction in PPG Signals Based on AS-LMS Adaptive Filter," IEEE Trans. Instrum. Meas. **61**(5), 1445–1457 (2012).
16. M. J. Hayes and P. R. Smith, "A New Method for Pulse Oximetry Possessing Inherent Insensitivity to Artifact," IEEE Trans. Biomed. Eng. **48**(4), 452–461 (2001).
17. M. S. Patterson, S. Andersson-Engels, B. C. Wilson, and E. K. Osei, "Absorption Spectroscopy in Tissue-simulating Materials: A Theoretical and Experimental Study of Photon Paths," Appl. Opt. **34**(1), 22–30 (1995).
18. J.-J. Kim, S.-P. Yang, D. Keum, and K.-H. Jeong, "Asymmetric Optical Microstructures Driven by Geometry-guided Resist Reflow," Opt. Express **22**(18), 22089–22094 (2014).
19. T. Durduran, R. Choe, W. B. Baker, and A. G. Yodh, "Diffuse Optics for Tissue Monitoring and Tomography," Rep. Prog. Phys. **73**(7), 076701 (2010).
20. F.-H. Huang, P.-J. Yuan, K.-P. Lin, H.-H. Chang, and C.-L. Tsai, "Analysis of Reflectance Photoplethysmograph Sensors," World Acad. Sci. Eng. Technol. **5**(11), 1266–1269 (2011).
21. A. Bjorgan, M. Milanic, and L. L. Randeberg, "Estimation of Skin Optical Parameters for Real-time Hyperspectral Imaging Applications," J. Biomed. Opt. **19**(6), 066003 (2014).
22. W. Fleming and D. P. Wesfall, "Adaptive Supersensitivity," in *Handbook of Experimental Pharmacology: Catecholamines I,* U. Trendelenburg, and N. Weiner ed. (Springer, 1988).

1. Introduction

Optical photoplethysmography (PPG) exhibits human vascular activity in a non-invasive and compact manner [1,2]. Reflection light from PPG sensors informs the pulsatile component of blood flow, directly related to the volume change of blood vessels. For instance, the blood volume increases in systolic phase and therefore the reflection decreases due to light absorption and vice versa in diastolic phase. PPG signals indicate two peaks of systolic and diastolic blood pressure signals for one single cycle and they give additional information for diverse vascular activities [3] such as the vessel elasticity [4], the stroke volume [5–8], the artery stiffness [9], the heart rate [10], and the capillary resistance [11]. However, the diastolic peaks become readily distorted due to the low signal-to-noise ratio (SNR) of reflection PPG sensors [12], which results from highly scattered light in turbid human tissue. The signal distortion still distracts the precise monitoring of diverse vascular activities except the heart rate of cardiac cycles, which is indicated by the pulse intervals in the reflection PPG monitoring.

Conventional noise reduction of reflection PPG signals can be achieved by either increasing the number of optoelectronic modules or employing the signal processing techniques. For instance, both two green and red light emitting diodes (LEDs) simultaneously provide different spectral signals to reduce low frequency motion artifacts [13]. In addition, MEMS accelerometers can be further implemented on PPG sensors to reduce the noise due to the motion artifact [14]. However, they still have some technical difficulties in either minimizing electrical power consumption or improving mechanical stability. In contrast, the signal processing methods utilize either the synthetic noise or the frequency domain analysis. The synthetic noise reference signals serve as an adaptive filtering process, where they are internally generated from the noise corrupted PPG signals and effectively utilized for the noise removal [15]. In addition, the frequency domain analysis cut off the noise signals over the 3rd fundamental frequency [16]. However, these methods increase the computational complexity and still hinder real-time monitoring.

Here we report an angle-selective optical filter (ASOF) for highly sensitive reflection PPG signal monitoring. The ASOF features slanted micromirror arrays embedded in transparent ultraviolet curable polymer resin on a glass substrate. LED light scattered within human tissue forms 'banana shape' as illustrated in Fig. 1(a) [17]. Ballistic or snake photons

Biomedical Optics EXPRESS

of reflection PPG signals follow the Snell's law and they inform human vascular activities whereas diffused photons lose the directionality due to the Mie scattering by the turbid tissue medium and therefore they act as the noise signals. The ASOF exhibits the controlled angular acceptance for backscattered LED light within human tissue following the Snell's law and thus reduces both the non-directional and the undesired noise signals prior to a photodetector. The optical transmittance can be set to half the maximum at normal incidence by precisely controlling the angle of micromirrors. As a result, the PPG signals of directional photons are efficiently collected within this acceptance angle by effectively blocking the noise with the ASOF.

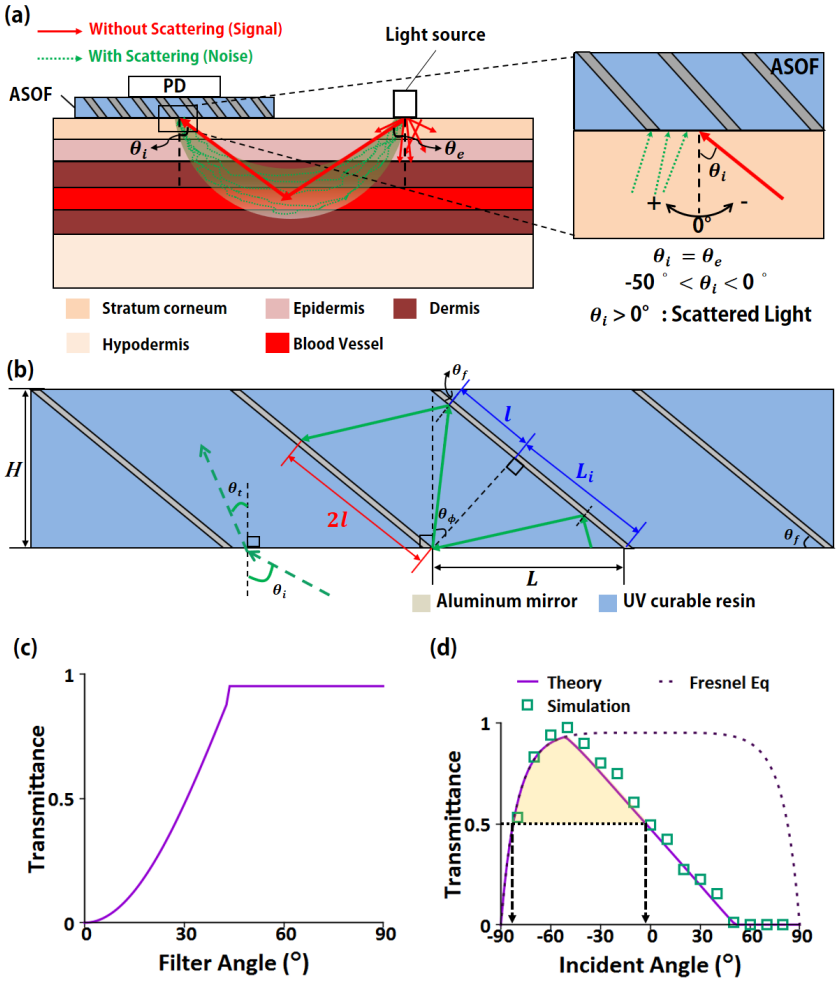

Fig. 1. Angle-selective optical filter (ASOF) for highly sensitive PPG sensors. (a) A schematic diagram of "banana" light shape under the human tissue. The red arrow is the light path followed by the Snell's law which has a PPG signal. The green arrow is the highly scattered light losing their directionality. The incident angle of light is distributed from 0 degree to LED's emitting angle. The incident light except these angle act as the noise of the PPG signals, which has low intensity and less information for vascular activity. (b) The cross-section of ASOF to calculate the transmittance, i.e., a ratio between the incident light and transmitted light area. The sum of *l* and Li is the incident light area and 2*l* is a transmitted light area. (c) The transmittance according to the filter angle when the incident angle of light is 0 degree. According to this result, the transmittance is set to half the maximum for the filter angle of 30 degrees. (d) Transmittance for the filter angle of 30 degrees depending on the incident angle. Both the theoretical and calculated results are in good agreement.

Biomedical Optics EXPRESS

2. Design and fabrication

Optical transmittance through the ASOF, i.e., a ratio between the incident and the transmitted light intensity, can be derived by using two dimensional ray analysis. Figure 1(b) depicts the cross-sectional view of ASOF. The aluminum (Al) of 500 nm in thickness and UV curable resin are chosen as reflecting and sustaining material for ASOF considering the high reflectivity and the practical fabrication procedures, respectively. The incident light intensity can be expressed as the length from the edge of the Al mirror to the point where the refracted light of the neighboring Al mirror reaches. The transmitted light intensity can also be represented by twice the length between the point where the refracted light of the neighboring Al mirror reaches and the point perpendicular to the edge of the adjacent Al mirror. The transmittance equation is given by

$$T = \begin{cases} 0, & l < 0 \\ \dfrac{2l}{L_i + l} F, & 0 \le l < L_i \\ F, & L_i \le l \end{cases}, \tag{1}$$

where, $l = L \cdot \sin\theta_f \cdot \tan\theta_\Phi$, $L_i = L \cdot \cos\theta_f$, $\theta_\Phi = \theta_f - \sin^{-1}[(n_1 \cdot \sin\theta_i / n_2)]$, θ_f is filter angle, θ_i is incident angle, and F is the transmittance using the Fresnel reflection as follows:

$$F = 1 - \frac{1}{2}\left(\left| \frac{n_1 \cos\theta_i - n_2 \sqrt{1 - \left(\frac{n_1}{n_2}\sin\theta_i\right)^2}}{n_1 \cos\theta_i + n_2 \sqrt{1 - \left(\frac{n_1}{n_2}\sin\theta_i\right)^2}} \right|^2 + \left| \frac{n_1 \sqrt{1 - \left(\frac{n_1}{n_2}\sin\theta_i\right)^2} - n_2 \cos\theta_i}{n_1 \sqrt{1 - \left(\frac{n_1}{n_2}\sin\theta_i\right)^2} + n_2 \cos\theta_i} \right|^2 \right). \tag{2}$$

From Eq. (1) and Eq. (2), the range of ASOF's acceptance angle can simply be designed by controlling the angle of slanted micromirrors embedded in ASOF. Here, the target filter angle is set to 30 degrees to have half the maximum transmittance at the normal incidence of light calculated from the numerical analysis described in Fig. 1(c). It was assumed in this calculation that the maximum reflectance of the Al mirror is one and the diffraction at the edge of the mirror was ignored as well. The equation is also confirmed by comparing with the numerical results in Fig. 1(d), where the simulated filter angle (θ_f) is 30° and the slanted microstructures are 10 μm in height (H) and 17 μm in length (L) in Fig. 1(b), respectively. Note that the length (L) and the height (H) of slanted Al mirror are controlled to have an appropriate mirror angle, irrelevant to the angular transmittance.

The microfabrication of ASOF was done by using resist reflowing and thermal evaporation as illustrated in Fig. 2(a). The slanted microstructures were simply defined by using the guided-resist reflowing method [18]. SU-8 (MicroChem) and AZ9260 (AZ Electronic Materials) served as thermoset and thermoplastic photoresist (PR). First, SU-8 was photolithographically defined as micropost structures on a 4-inch silicon (Si) wafer, where a thin SU-8 base layer served as an adhesion layer between SU-8 and the bare silicon. Next, AZ9260 was defined on the predefined SU-8 microstructures. Both the microstructures were thermally annealed, where AZ9260 microstructures steadily reflowed along the geometric boundaries of SU-8 microstructures. The slanted microstructures were transferred to polydimethylsiloxane (PDMS) and then replicated to an UV curable optical adhesive resin (NOA 63, Norland Products Inc.) on a glass substrate. The optical resin replica was thermally deposited with a thin Al layer, which served as micromirror arrays. UV curable resin as an index matching spacer was refilled, pressurized, and cured in the interstitial spacing between the slanted microstructures and the glass substrate. Figure 2(b) and 2(c) show the scanning electron microscope (SEM) images of slanted microstructures on a silicon wafer. Figure 2(d)

Biomedical Optics EXPRESS

also displays that thin Al micromirrors are clearly formed on the inclined surface of slanted microstructures. Note that the side walls of the slanted microstructures are not covered with thin Al film due to a slight negative angle of the SU-8 microposts and therefore they allow light transmission near the filter angle after the embedment of micromirrors with additional UV resin.

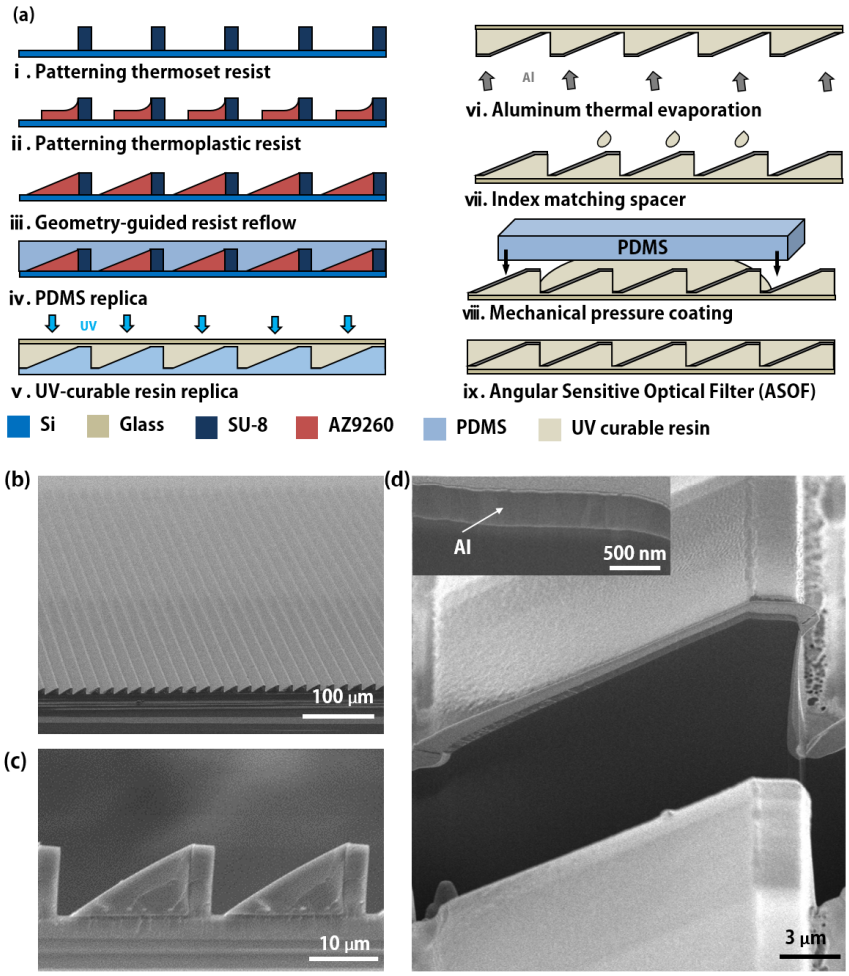

Fig. 2. (a) Microfabrication procedure of the ASOF. SU-8 line patterns as a thermoset post were initially patterned on a Si wafer. The slanted microstructures with a target filter angle were then formed on the Si wafer by using the geometry-guided resist reflow method. The microstructures were transferred onto UV curable resin on a cover glass by using the PDMS replica and then A 500nm thick Al film was thermally evaporated on the replicated slanted microstructures. The slanted micromirrors were finally embedded in UV resin. (b) The perspective and (c) cross-sectional SEM images of slanted microstructures. The slanted microstructures are 10 μm in height and 17 μm in length and therefore they provide the filter angle of 30 degrees after the Al evaporation. (d) A perspective SEM image of the Al micromirror after focused ion-beam cut. Note that the side walls of the micromirrors are not covered with thin Al film and therefore still transparent after the embedment of micromirrors with additional UV resin.

3. Angle-selective optical filter (ASOF) based PPG sensor

The ASOF can effectively accept ballistic and snake photons scattered from human tissue. The angle-selectivity was measured by using a rotatable integrating sphere as illustrated in

Biomedical Optics EXPRESS

Fig. 3(a). A 533 nm laser beam was injected onto the ASOF after a 3 mm pinhole, which was placed on the entrance hole of an integrating sphere.

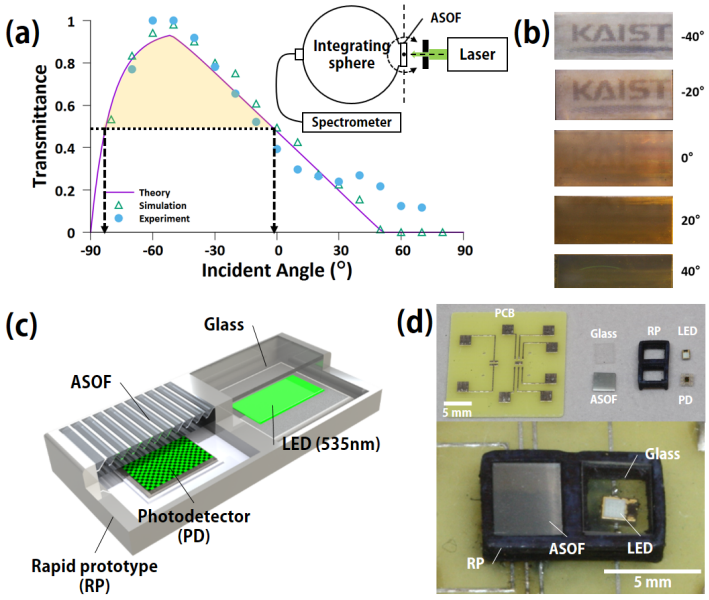

Fig. 3. (a) Light transmittance through the ASOF depending on an incident angle of 533 nm laser beam. The angular transmittance was measured with an integrating sphere rotating with respect to the ASOF. The experiment results are in good agreement with the calculated and theoretical results. However, the transmittance of ASOF shows a significant difference more than an incident angle of 50 degrees due to the optical diffraction from the Al micromirror arrays. (b) A transmitted image captured via ASOF rotating in front of "KAIST" text printed on white paper (see Visualization 1). (c) A schematic diagram of ASOF based PPG sensor. The ASOF on the PD was simply replaced with a glass window for the comparison between PPG sensors with and without the ASOF. (d) An optical image of a fully packaged PPG sensor consisting of PD, LED, RP and PCB.

The incident angle was precisely controlled by simultaneously rotating both the ASOF and the integrating sphere. The transmittance of the ASOF was numerically calculated by using BRO (Breault Research Organization) BIOToolkit for ray-tracing based optical simulation software ASAP (Advanced System Analysis Program, BRO), depending on an incident angle of light. Human tissue was modeled as a volume scatter that has the absorption coefficient, the scattering coefficient, and the anisotropy factor. For this tissue model, the stratum corneum was 7.5 μm, the epidermis was 43 μm, the upper dermis was 0.25 mm, the lower dermis was 2.25 mm, and the hypodermis was 3 mm in thickness. In this calculation, the pulsatile component of PPG signals was considered as the variation of the blood volume fraction (BVF) of the upper dermis, varying from 0.02% to 5%. The peak-to-peak values of PPG signals were defined as the intensity difference between the 0.02% and 5% of BVF and the DC noise was also defined by the average of the peak-to-peak values of PPG signals. Figure 3(a) successfully demonstrates the ASOF accepts the scattered light from - 90 to 50 degrees with cutoff angles at near 0 and −80 degrees. The experiment results are well matched with both the theoretical and the numerical results. Due to the light diffraction occurring at the interstitial spacing between the micromirror arrays, both the results show the transmittance is not zero but still low over an incident angle of 50 degrees. Figure 3(b) shows the transmitted optical images through the ASOF rotating prior to 'KAIST' text printed on a white paper, where the image brightness clearly depends on the incident angle. Figure 3(c) shows the schematic illustration of a ASOF based PPG sensor. The gap between photodiode

Biomedical Optics EXPRESS

and LED was set to 1.3 mm, considering the relationship that the gap is roughly twice of the penetration depth of light in the reflection geometry [19]. For this particular case, the penetration depth was around 300 μm to detect the pulsatile component of human tissue. The target penetration depth was set to 650 μm by considering the irregular thickness of the dermis layer on the measurement site. Figure 3(d) shows the fully assembled PPG sensor, which consists of a photodiode, a 535 nm LED, a printed circuit board (PCB), and a plastic housing part manufactured by a 3D rapid prototyping (RP) printer. The RP was then painted in black to reduce unwanted reflection inside the package.

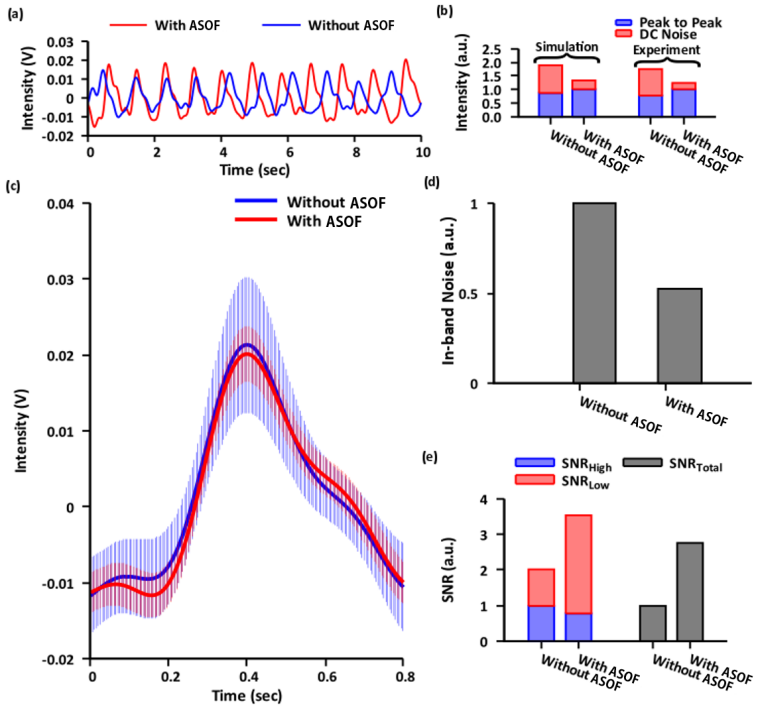

Fig. 4. (a) PPG signals after passing a bandpass filter of 0.5 Hz to 4 Hz. ASOF has little effect on the peak-to-peak value of the PPG signals. (b) Comparison of the experimental and the numerical results for peak-to-peak signals and DC noise of PPG signals. In both cases, ASOF clearly reduces DC noise by more than three times. (c) Ensemble averaged PPG signals. ASOF clearly indicates the diastolic peaks of PPG signals. The variation of the PPG signals, indicated by the error signals, indicates the in-band noise of the PPG signals, i.e. the sum of error signals. (d) In-band noise of PPG signals. ASOF reduces the in-band noise by twice. (e) Signal-to-noise ratio (SNR), defined as ratio of the power spectral density (PSD) of PPG signal and PSD of the noise in raw data. PSD_{Signal} is the PSD of the PPG signal, and PSD of noise such as PSD_{High} and PSD_{Low} are the PSD of the higher and lower frequency noise than PPG signal, respectively. The SNR of the PPG signal is defined as the ratio between PSD_{Signal} and the PSD of the noise, such as PSD_{High} and PSD_{Low}. According to this definition, ASOF improves SNR more than three times.

The PPG signals were measured by using LabVIEW and National Instrument USB-6009 data acquisition device. The sampling frequency was 200 Hz and the data acquisition time was 10 sec. The LED (LXZ1-PM01, LUMILEDS) and PD photodetector (ISL29101, Intersil) were applied at 3 V_{DC} and 2.5 V_{DC}, respectively. The PPG signals were measured on the forearm and analyzed by using MATLAB. The PPG signals were distributed in the frequency range of 0.5 Hz to 4 Hz whereas the high frequency noise ranges from 4 Hz to 100 Hz and the low frequency noise from 0 Hz to 0.5 Hz. The in-band noise of PPG signals was calculated by taking the sum of the standard deviation for PPG signals of 500 waveforms on each cases. Figure 4(a) displays the measured bandpass PPG signals for 0.5 Hz to 4 Hz from

Biomedical Optics EXPRESS

both the PPG sensors [20]. The measured peak-to-peak PPG signals are hardly affected by the ASOF and they are well matched with the calculated results based on a ray-tracing software ASAP, where the pulsatile components of PPG signals were considered as the variation in blood volume fraction (BVF) of upper dermis [21]. The calculated results also show the DC noise and the peak-to-peak values of PPG signals, where the DC noise is defined as an average of the peak-to-peak values and the peak-to-peak values were obtained as the BVF varies from 0.2% to 5% [22]. As shown in Fig. 4(b), both the results clearly indicate the DC noise for PPG sensor with the ASOF is three times smaller than that without the ASOF. The PPG signals through the ASOF were further analyzed by using the ensemble averaging technique. The ensemble average was calculated by finding the systolic peak, extracting a 0.8 sec long waveform around the systolic peak, summing the waveforms, and averaging. Figure 4(c) shows the ensemble averaged PPG signals of 60 samples for 10 seconds for each case. The ASOF clearly indicates the diastolic peak due to the reduction of the in-band noise overlapping the signal bandwidth. The calculation of the in-band noise uses the standard deviation (STD) of the PPG signals, which represent the signal variation. In addition, the sum of the STDs is the quantitative total in-band noise of PPG signals. Figure 4(d) shows that the total in-band noise with ASOF is two times smaller than that without ASOF. Figure 4(e) shows the result of calculating the power spectral density (PSD) ratio for the bandwidth of the raw data. PSD_{Low} and PSD_{High} are PSDs with bandwidths higher or lower than PPG signals, respectively, and PSD_{Signal} is the PSD of PPG signals. The SNR is defined as the ratio between PSD_{Signal}, i.e., and the PSD of the noise such as PSD_{High} and PSD_{Low}. In other words, SNR_{Low} is PSD_{Signal}/PSD_{Low} and SNR_{High} is PSD_{Signal}/PSD_{High} and SNR_{Total} is $PSD_{Signal}/(PSD_{Low} + PSD_{High})$. The experimental results clearly show that the PPG sensor with ASOF has the SNR_{Low} and SNR_{Total} three times higher than that without ASOF due to the reduction of the low-frequency noise of the raw data.

4. Conclusions

In summary, this work has successfully demonstrated the angle-selective optical filter for highly sensitive reflection PPG sensors. The ASOF selectively transmit or block the light, depending on an incident angle of light. The optical filter was designed by using the ray-tracing analysis and then successfully fabricated through microfabrication procedures. The experimental results clearly show that optical transmittance through the ASOF changes with the filter angle, which was determined by the inclined angle of Al micromirror arrays. Besides, the ASOF also significantly reduces the in-band noise and low frequency noise of PPG signals. Compared to conventional PPG sensors, the ASOF based PPG sensor safely preserves the waveform of PPG signals due to the efficient reduction of low frequency noise, which occurs at the smaller angles than the reflection angle. As a result, the diastolic peaks clearly appear in the PPG signals with the ASOF. This new optical filter offers a new opportunity for highly sensitive PPG monitoring or diffuse optical imaging on turbid medium such as human tissue.

Funding

This work was supported by the National Research Foundation of Korea (2016013061, 2016924609, 2016919193), funded by the Ministry of Science, ICT & Future Planning, and a grant of the Korean Health Technology R&D Project through the Korea Health Industry Development Institute (KHIDI), funded by Ministry of Health & Welfare, Republic of Korea (grant number: HI13C2181, HI16C1111) and the research project of Samsung Electronics, Inc.

Disclosures

The authors declare that there are no conflicts of interest related to this article.